Available online at www.sciencedirect.com
ScienceDirect
Remote Sensing of Environment 106 (2007) 228–237
Remote Sensing of Environment
www.elsevier.com/locate/rse

Predicting temperate conifer forest successional stage distributions with multitemporal Landsat Thematic Mapper imagery

Conghe Song [a,*], Todd A. Schroeder [b], Warren B. Cohen [c]

[a] Department of Geography, CB# 3220, 205 Saunders Hall, University of North Carolina at Chapel Hill, Chapel Hill, NC 27599, USA
[b] Department of Forest Science, Oregon State University, Corvallis, OR 97331, USA
[c] Forestry Sciences Laboratory, Pacific Northwest Research Station, USDA Forest Service, 3200 SW Jefferson Way, Corvallis, OR 97331, USA

Received 15 January 2006; received in revised form 24 August 2006; accepted 27 August 2006

Abstract

Forest succession is a fundamental ecological process which can impact the functioning of many terrestrial processes, such as water and nutrient cycling and carbon sequestration. Therefore, knowing the distribution of forest successional stages over a landscape facilitates a greater understanding of terrestrial ecosystems. One way of characterizing forest succession over the landscape is to use satellite imagery to map forest successional stages continuously over a region. In this study we use a forest succession model (ZELIG) and a canopy reflectance model (GORT) to produce spectral trajectories of forest succession from young to old-growth stages, and compared the simulated trajectories with those constructed from Landsat Thematic Mapper (TM) imagery to understand the potential of mapping forest successional stages with remote sensing. The simulated successional trajectories captured the major characteristics of observed regional mean succession trajectory with Landsat TM imagery for Tasseled Cap indices based on age information from the Pacific Northwest Forest Inventory and Analysis Integrated Database produced by Pacific Northwest Research Station, USDA Forest Service. Though the successional trajectories are highly nonlinear in the early years of succession, a linear model fits well the regional mean successional trajectories for brightness and greenness due to significant cross-site variations that masked the nonlinearity over a regional scale ($R^2=0.8951$ for regional mean brightness with age; $R^2=0.9348$ for regional mean greenness with age). Regression analysis found that Tasseled Cap brightness and greenness are much better predictors of forest successional stages than wetness index based on the data analyzed in this study. The spectral history based on multitemporal Landsat imagery can be used to effectively identify mature and old-growth stands whose ages do not match with remote sensing signals due to change occurred during the time between ground data collection and image acquisition. Multitemporal Landsat imagery also improves prediction of forest successional stages. However, a linear model on a stand basis has a limited predictive power of forest stand successional stages (adjusted $R^2=0.5435$ using the Tasseled Cap indices from all four images used in this study) due to significant variations in remote sensing signals for stands at the same successional stage. Therefore, accurate prediction of forest successional stage using remote sensing imagery at stand scale requires accounting for site-specific factors influence remotely sensed signals in the future.

Keywords: Forest succession; Stand age; Multitemporal Landsat Imagery; ZELIG; GORT

1. Introduction

Covering nearly a third of the Earth's land area, forests play a critical role in global terrestrial ecosystems, including, but not limited to, providing a temporary carbon sink in the global carbon cycle (Dixon et al., 1994; Goodale et al., 2002; Wofsy et al., 1993), preservation of biodiversity (Dobson et al., 1997) and conservation of soil and water resources (Lal, 1997; Woo et al., 1997). Moreover, forest successional stages strongly influence the functions of terrestrial ecosystems (Chen et al., 2002; Cohen et al., 1995; Foody et al., 1996; Pregitzer & Euskirchen, 2004; Song & Woodcock, 2003a). Therefore, to gain greater insight into understanding terrestrial ecosystem processes, we need to generate accurate information regarding the extent of forests and forest successional stages.

* Corresponding author. Tel.: +1 919 843 4764; fax: +1 919 962 1537.
E-mail address: csong@email.unc.edu (C. Song).

0034-4257/$ - see front matter © 2006 Elsevier Inc. All rights reserved.
doi:10.1016/j.rse.2006.08.008

A traditional approach to estimate forest successional stage is through fieldwork. Although accurate, this approach can be costly, as well as limited in scope, as it only provides successional stage information for a limited number of stands at the landscape scale. Remote sensing offers the potential to efficiently extend field based measurements of forest successional stage to large geographic areas in a repeated manner. Although remote sensing has proven successful in mapping deforestation due to the dramatic change in spectral reflectance occurring after forest removal (Cohen et al., 1998; Pax-Lenney et al., 2001; Skole & Tucker, 1993), mapping forest successional stages remains a challenge due to the subtle reflectance changes associated with forest succession in optical imagery. Most existing remote sensing studies on mapping forest successional stages are based on classification of a single date image into a few broad successional classes (Fiorella & Ripple, 1993; Hall et al., 1991; Jakubauskas, 1996; Kimes et al., 1996). Some studies have incorporated multiple images in deriving forest successional stages, however each image was classified independently and used post-classification comparison to identify the starting date of forest regeneration (Foody et al., 1996; Lucas et al., 2002). Therefore, a more synergistic approach to use multitemporal satellite imagery to predict forest successional stage distributions could have great merit.

Thus, our two objectives in this study are to more fully understand how the spectral properties of forests change from young to mature to old-growth stages, as well as to predict forest successional stages from multitemporal imagery. We accomplish our first objective by generating temporal trajectories of forest succession in the spectral space by coupling a forest succession model (ZELIG) (Urban, 1990) with a forest canopy reflectance model (GORT) (Li et al., 1995). These simulated temporal patterns of forest succession are then compared with successional patterns based on Landsat imagery and ground based forest age class data collected by U.S. Forest Service Pacific Northwest (PNW) Forest Inventory and Analysis (FIA) program. Finally, we accomplish our second objective by using multiple regression techniques to study the synergistic value of predicting detailed forest age classes with multitemporal Landsat images.

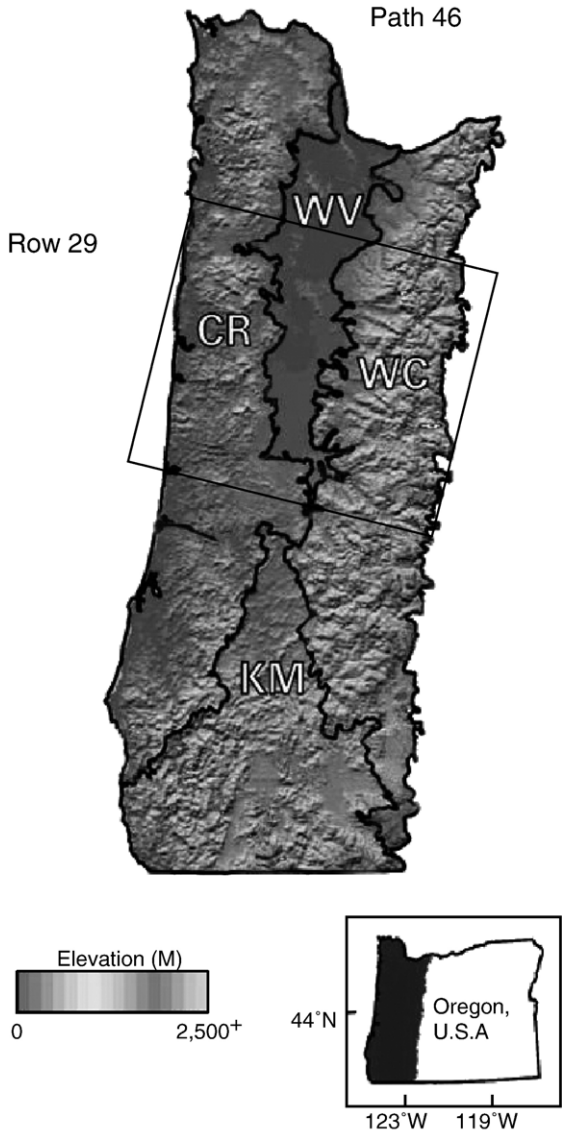

Fig. 1. Study area is WRS path/row=46/29 encompassing Western Cascades (WC), Coastal Ranges (CR), and the Willamette Valley (WV).

2. Methodology

2.1. Study area and data

The study area is located in western Oregon and falls within WRS path/row 46/29 (Fig. 1). The area encompasses three geographic provinces, which include the Western Cascades (WC), Willamette Valley (WV), and Coastal Range (CR) provinces (Cohen et al., 2002). Forest stand age distribution classes were derived from the PNW-FIA Integrated Database version 1.4 (Hiserote & Waddell, 2004). The FIA ground data were collected on 2.1 hectare plots in a diamond shape during the 1995 (1995–1997) periodic forest inventory of western Oregon. For each plot, stand age was coded into one of 22 age classes as shown in Table 1. Since FIA plot locations are confidential, the spectral data for each field plot within our study area was extracted through special arrangement with the Pacific Northwest Research Station, USDA Forest Service. The accuracy of the database with respect to plot locations is unknown, and is variable among plots. Using level 1G Landsat data, the digital numbers (DN) for each FIA plot within the study area was extracted using the average DN of a 22 pixel window that cover the sampling plot. A total of 2441 FIA plots fell within Landsat path/row 46/29, however only 1154 conifer dominated plots with uniform age class condition that fall in western Cascades and the Coastal Ranges were used in our study.

Spectral relationships were derived in this study using four near anniversary Landsat 5 TM images acquired on 04 August 1984, 07 July 1991, 31 July 1994 and 23 July 1997, respectively. Noise effects due to differences in sun angle and phenology were minimized given the similarity in acquisition date (Song & Woodcock, 2003b).

Table 1
Forest stand age classes as coded in the integrated database version 1.4 compiled by the Pacific Northwest Forest Inventories and Analysis program

Age class	Stand ages (years)
1	0–9
2	10–19
3	20–29
4	30–39
5	40–49
6	50–59
7	60–69
8	70–79
9	80–89
10	90–99
11	100–109
12	110–119
13	120–129
14	130–139
15	140–149
16	150–159
17	160–169
18	170–179
19	180–189
20	190–199
21	200–300
22	300+

Ground data were collected during 1995–1997 for western Oregon.

2.2. Image preprocessing

Two critical preprocessing steps were applied to the images: geometric registration and atmospheric correction. Due to the nature of analysis taken in this study, a high accuracy of image-to-image registration was required. Thus, we used a semi-automatic image-to-image registration program originally developed at Boston University. The program minimizes the manual work in collecting ground control points (GCP) by identifying a large number of GCPs with low root mean squared error (RMSE). All the images in this study were registered to a master reference image with RMSE under 0.3 pixels using 50 or more GCPs.

Correction for atmospheric effects is a complicated issue. Though many algorithms have been developed (Chavez, 1996; Liang et al., 1997; Schott et al., 1988; Song et al., 2001), it is highly debatable with respect to which atmospheric correction algorithm produces the most accurate surface reflectance, particularly for algorithms based on images without *in-situ* atmospheric data. Here we use the modified dense dark vegetation (DDV) algorithm based on its effectiveness in a previous study (Song & Woodcock, 2003b). DDV is based on the theoretical relationship between the surface reflectance of dense dark vegetation in TM bands 1, 3, and 7 proposed by Kaufman et al. (1997) as

$$\begin{cases} \rho_1 = 0.25\rho_7 \\ \rho_3 = 0.5\rho_7 \end{cases} \quad (1)$$

where ρ_1, ρ_3 and ρ_7 are the surface reflectance for TM bands 1, 3 and 7. The theory was implemented by Liang et al. (1997) on a moving window basis. The DDV algorithm was modified (MDDV) by Song et al. (2001) for operational use. In a comparative study by Song and Woodcock (2003b), MDDV produces surface reflectances similar to those produced by the 6S algorithm (Vermote et al., 1997) using observed atmospheric data as input. The effects of sensor degradation on Landsat 5 images were accounted for using the approach of Song et al. (2001).

After conversion of DNs to surface reflectances, we further transformed the 6 TM bands for each image to brightness, greenness and wetness using the Tasseled Cap transformation (Kauth & Thomas, 1976). We used the coefficients of Crist (1985) in the transformation. Since multispectral remotely sensed data are typically correlated across bands there is a tremendous amount of information redundancy contained within the six reflective TM bands. Thus, the Tasseled Cap transformation can be used to significantly reduce the amount of data processing, particularly for multitemporal images, without significant loss of spectral information for the forest conditions of interest (Cohen et al., 1995).

2.3. Simulation of forest succession in optical imagery

To gain a theoretical understanding of the manifestation of forest succession in optical imagery, we first simulated the changes in spectral properties over the course of forest succession. The simulation was accomplished in two steps. First, the ZELIG model (Urban, 1990) was used to simulate the growth of a stand with time. Second, canopy structure was then extracted from the stands generated by ZELIG and used as input to the GORT canopy reflectance model (Li et al., 1995).

ZELIG is a generalized version of a large group of models, referred to as gap models. The size of the plot simulated by a gap model is equivalent to the size of the canopy of a full grown individual. At this spatial scale the model emphasizes the ecological roles of gaps produced by the death of existing individuals. JABOWA was the first gap model originally developed by Botkin et al. (1972). JABOWA was modified to become FORET by Shugart and West (1977). JABOWA and FORET have since become the basis for dozens of other gap models developed for different forest ecosystems, including ZELIG. ZELIG simulates three critical ecological processes in forest ecosystems at an annual time step: growth, establishment and mortality, each of which is constrained by light availability, temperature, soil moisture and fertility. The growth of each individual within a plot without environmental constraint, i.e. optical growth, is simulated as

$$\frac{dD}{dt} = \frac{GD(1-DH/(D_{max}H_{max}))}{274 + 3b_2D - 4b_3D^2} \quad (2)$$

where G is a species-specific growth factor. D_{max} and H_{max} are species-specific maximum diameter at breast height (DBH) and maximum height. D is the current DBH, and H is the current height. The species-specific parameters of b_2 and b_3 are used to estimate tree height as: $H = 137 + b_2D - b_3D^2$, and they are related to D_{max} and H_{max} as: $b_2 = 2(H_{max} - 137)/D_{max}$ and $b_3 = (H_{max} - 137)/D^2_{max}$. The actual growth of DBH in ZELIG is

optimal growth after environmental constraints applied as: $\Delta D = f(L) * \min(f(M), f(F)) * f(T) * \Delta D_{opt}$, where $f(L)$, $f(M)$, $f(F)$ and $f(T)$ are scalars between 0 and 1 due to suboptimal conditions from light, soil moisture, soil fertility and temperature, respectively. Establishment of new individuals is simulated stochastically based on species-specific potential establishment rate modified by environmental constraints similar to optimal growth. Tree mortality is also simulated as a stochastic process, arising from two sources: natural mortality and that from environmental constraint. Natural mortality is simulated based on the assumption that 1% of individuals survive to reach the species-specific maximum age. Mortality caused by stress is based on the assumption that only 1% of the stressed individuals will survive for 10 years.

GORT is a hybrid of geometric optical and radiative transfer models, simulating reflectance of forest canopies for a given illumination and viewing geometry (Li et al., 1995). The geometric optical model (Li & Strahler, 1985, 1992) accounts for the discrete nature of forest canopies based on stem density, tree crown size and shape. The geometric optical model provides careful quantification of single scattering of photons in the canopy and captures the fundamental properties of forest canopy bidirectional reflectance distribution function (BRDF). Multiple scattering between canopy elements, which is highly simplified in the geometric optical model, is simulated by the model based on radiative transfer theory. Therefore, GORT is capable of accounting for varying degrees of discreteness in the forest canopy. The discrete nature of forest canopies is represented by two types of gaps in GORT: the between- and within-crown gap probabilities. The between-crown gap probability is modeled based on Boolean set theory (Serra, 1980) as

$$P(n = 0|h, \theta) = e^{-\lambda V(h,\theta)} \quad (3)$$

where n is the number of tree crowns that a beam of sunlight passing through; h and θ are height and sun zenith angle. $V(h,\theta)$ is the volume of tree crowns that sunbeam passes through a thin layer at height h from zenith angle θ. The within-crown gap probability is based on the path length that a sunbeam passing through tree crowns, and is simulated as

$$P(\mathrm{n}>0|h, \theta) = \int_0^\infty P(s|h, \theta) e^{-\tau(\theta)s} \mathrm{d}s \quad (4)$$

where s is the path-length of a sunbeam passing through the crown at height h and zenith θ. The extinction coefficient from zenith θ is estimated as: $\tau(\theta) = KL/H$, where K is the attenuation of a unit leaf area index contained within a unit canopy depth. L is the leaf area index, and H is the average canopy depth. $P(s|h, \theta)$ is the probability distribution function of path-length at height h and zenith θ.

Canopy structure parameters derived from ZELIG used as input to GORT are given in Table 2. They include the upper and lower boundaries of crown center heights, stem density, average horizontal crown radius, and foliage area volume density. The simulation of stand development in ZELIG starts from bare ground and proceeds up to 250 years following Urban et al. (1993) for H. J. Andrews Experimental Forest (HJA). The simulation is conducted for 50 independent plots, and the canopy structure parameters are extracted from all trees within the 50 plots. Due to the complexity of forest canopies for mature and old-growth forests, a single layer canopy cannot adequately represent the stand structure. In this study, we used two layers to represent the canopy: the overstory and the understory. The overstory is composed of individuals that add up to 80% of total crown volume in the top of the canopy, while the remaining individuals belong to the understory. Separate canopy structural parameters (Table 2) are extracted from the individuals belonging to each layer. The canopy reflectance of the understory layer is simulated first. The understory canopy reflectance is then used as the background reflectance when simulating canopy reflectance for the overstory. Due to the fact that forests in this region are predominately coniferous, we also assume that all trees in the plots are conifers sharing the same elongated ellipsoid crown shape as the current version of the GORT model does not support mixed crown shape in a stand.

Table 2
Canopy structure parameters extracted from stands simulated by ZELIG used as input to GORT to simulate canopy reflectance as the stand develops

Symbols	Values
h_1	Upper boundary of crown center height (m)
h_2	Lower boundary of crown center height (m)
R	Average crown horizontal radius (m)
λ	Stem density (trees/m^2)
FAVD	Foliage area volume density (m^2/m^3)

In addition to the structural complexity associated with the spectral manifestation of stand successional stages, the canopy spectral properties also change according to the presence of dead leaves and branches, mosses and lichens present in the upper canopy (Cohen et al., 1995). Unfortunately these impacts on canopy reflectance are not explicitly incorporated in GORT since leaves within a tree crown are treated as a turbid medium. Thus, to more accurately account for the effects of dead leaves, branches, mosses and lichens in the canopy we change the "leaf" spectral properties gradually so they more realistically resemble the changes associated with forest succession. The "leaf" spectral properties for old-growth forests were derived from an old-growth stand identified from the TM image. We then linearly interpolated the leaf spectral properties from a young closed canopy to those of old-growth stands between 51 and 250 years old.

2.4. Statistical analysis

We conducted a statistical analysis to understand whether multiple images facilitate our ability to predict successional stage information derived from Landsat imagery. The following multiple linear regression model was used to assess the relationship between stand age classes and multitemporal spectral measurements:

$$y = b_0 + b_1 x_1 + b_2 x_2 + \ldots + b_n x_n + \varepsilon \quad (5)$$

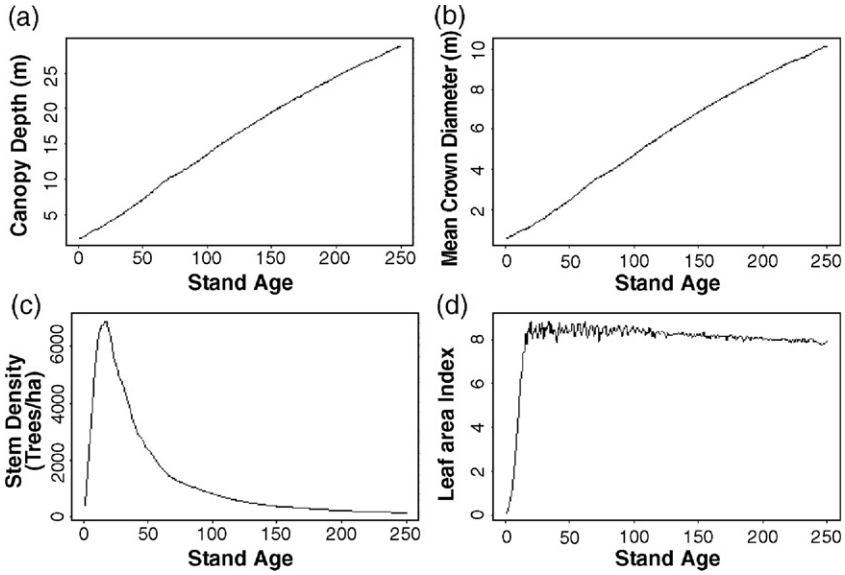

Fig. 2. Change of overstory canopy structure as simulated with ZELIG model for the H. J. Andrews Experimental Forest over 250 years. The simulation is conducted for 50 independent plots. The canopy structure parameters shown here are the mean values averaged over all plots simulated.

Where y is the stand age class obtained from the FIA plots, and x_i are the Tasseled Cap transformation indices. The error term is ε. Although age is coded in discrete classes in the original dataset, it can be treated as a numerical variable since the age class numbers are proportional to stand ages measured on the ground (Table 1). The coefficients b_i of x_i represent the rate and direction of changes in the spectral domain given a specific stand age. Therefore, the multiple linear regression model as described in Eq. (5) can capture some nonlinear changes in spectral properties associated with changes in forest succession through time. Therefore, it is expected that there will be a stronger statistical relationship or a higher adjusted R-square value with Eq. (5) using multiple images than using a single date image. Here we compare regression outputs using the adjusted R-square statistic in order to account for the effect of different numbers of independent variables in the predictive models. We expect that using more images at different times in the regression model will result in higher adjusted R-squares as adding additional independent variables will allow for the explanation of a higher percentage of variation in successional stage distribution classes.

3. Results

3.1. Simulated successional trajectories

The change in overstory canopy structure with time as simulated by ZELIG is shown in Fig. 2. The simulation was not calibrated to any particular stand, but the available species, climate and soil were set to conditions typically found at HJA. The simulation captured the temporal pattern of biomass accumulation well in the region (Song & Woodcock, 2003a). The depth of canopy (Fig. 2a), which is the difference between the upper and lower boundaries of the canopy, increases almost linearly with time. A similar trend is also found for the mean crown diameter (Fig. 2b) in the overstory as both are ultimately derived from DBH. However, the change of stem density with time is highly nonlinear (Fig. 2c). It increases rapidly with time to reach a maximum density around 20 years, which approximates the time of canopy closure. At this point in stand development the self-thinning process begins, which results in a decrease in the number of individuals found in the overstory canopy. While leaf area index of the overstory reaches its maximum value at roughly the same time as stem density (Fig. 2d), the peak in leaf area index is maintained with only a slight decreasing trend, while stem density decreases rapidly. The asymptotic peak observed in leaf area index indicates that the decrease in stem density is likely the result of small trees being replaced with fewer larger ones.

Assuming that the simulation by ZELIG provides a general pattern of canopy structure change over the course of forest succession, we generated successional trajectories in the

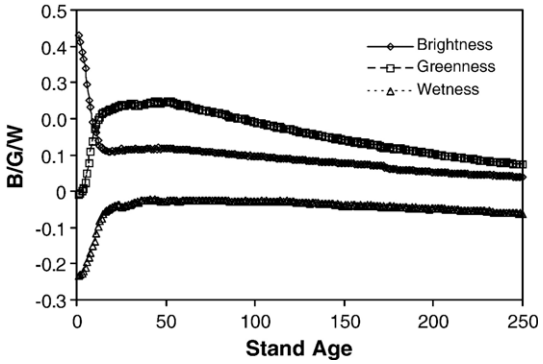

Fig. 3. Simulated trajectory of brightness, greenness and wetness of Tasseled Cap transformation with stand age. The succession of the stand was simulated with ZELIG, and the output of ZELIG was used as input to the GORT model to simulate the canopy reflectance in six reflective bands of Landsat TM sensors. The simulated TM reflectance is processed with Tasseled Cap transformation.

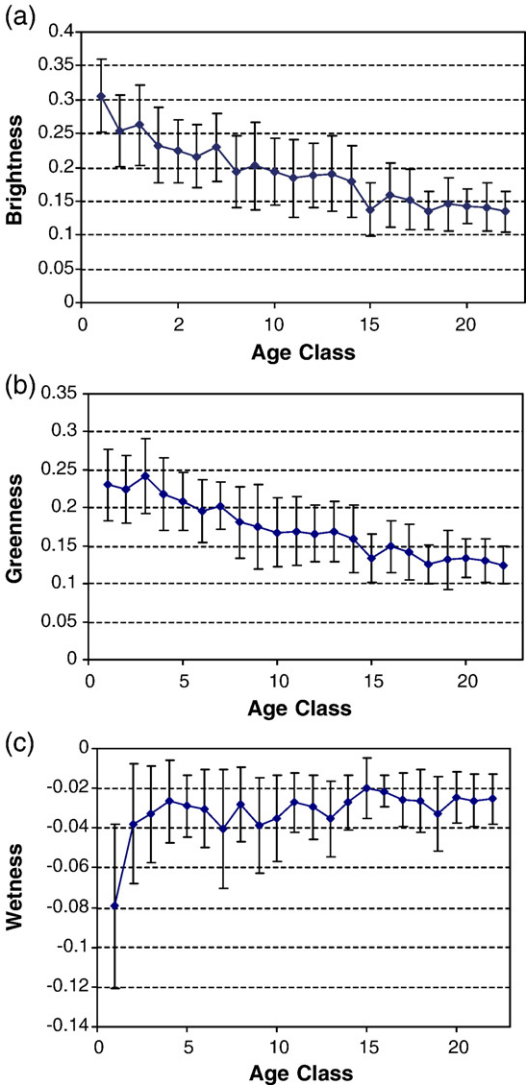

Fig. 4. Observed trajectory of brightness, greenness and wetness of Tasseled Cap transformation with stand age from FIA plots in the 1997 image. Each point is the mean value from all plots within the age class, and the vertical error bars are ± 1 SD. The simulated trajectories in Fig. 3 captured the major characteristics of the observed trajectories here. (a) Regional mean successional trajectory of brightness; (b) regional mean successional trajectory of greenness; (c) regional mean successional trajectory of wetness.

spectral space with GORT (Fig. 3). All three simulated Tasseled Cap trajectories change rapidly during early years in succession (<20 years) and much slower once the canopy closes. Brightness decreases with stand age rapidly as the simulation starts on a bright, bare background. The establishment of trees quickly decreases the brightness of the scene, and once the canopy approaches closure, the decrease in brightness is much slower. Greenness increases very fast with establishment of new individuals on the background, and maximizes around 30–50 years old, after which it begins to slowly decrease. Wetness increases quickly to its maximum value, then stays almost at this maximum with a slight decrease toward the old-growth stage. The observed decrease in all three Tasseled Cap indices as the stand matures is the result of the combined effect of both structural and spectral changes in the canopy. As the stand becomes older, there are larger and fewer individuals in the overstory (Fig. 2), creating more shadows in the canopy and possessing more dead leaves and branches and mosses and lichens, which causes decrease in Tasseled Cap indices.

3.2. Observed successional trajectory

To evaluate how well our simulated spectral trajectories capture changes associated with forest succession in the real world, we now develop spectral successional trajectories for stands with age data collected by FIA. Since FIA ground plots were measured over the course of 3 years (1995–1997) (Hiserote & Waddell, 2004), we elected to use the 1997 image, as it best matches with the recorded age information. In addition, we have to use stands at different ages at different locations, i.e. substitute time with space, in order to construct a successional trajectory from young to old-growth as it is impossible to do so with a single stand. Since topographic effects have been found to impact successional trajectories developed from satellite imagery (Song et al., 2002), we eliminate stands on steep slopes (>30°) and high elevation sites (>1000 m) from the analysis. Because the ZELIG simulation was not calibrated to any one particular stand, we cannot directly compare the simulated successional trajectories at the stand level. Thus, we pooled all the FIA plots and calculated mean Tasseled Cap trajectories

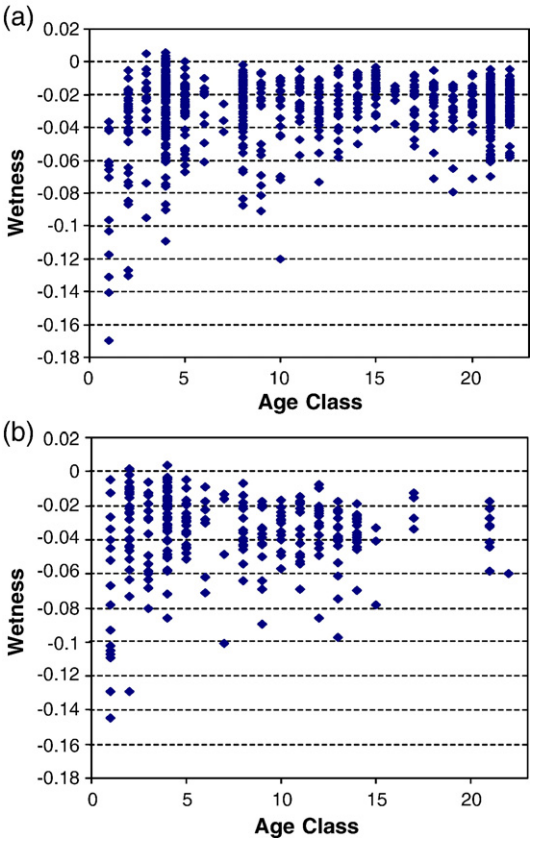

Fig. 5. Spectral trajectory of wetness separated for (a) western Cascades and (b) Coastal Ranges. The decreasing trend of wetness from mature to old-growth is much clearer when the two ecoregions are viewed separately than view together as seen in Fig. 4c.

Table 3
Results of multiple regression analysis between age classes and brightness (B), greenness (G) and wetness (W) indices from 1984, 1991, 1994 and 1997 Landsat 5 TM images for all plots after screening

Variables	R^2	Adj R^2	P-value
B1	0.2615	0.2600	0.0001
B2	0.2785	0.2755	0.0001
B3	0.2951	0.2906	0.0001
B4	0.3104	0.3046	0.0001
G1	0.2895	0.2879	0.0001
G2	0.3222	0.3193	0.0001
G3	0.3344	0.3302	0.0001
G4	0.3437	0.3382	0.0001
W1	0.0249	0.0229	0.3086
W2	0.0646	0.0607	0.0517
W3	0.0996	0.0939	0.0006
W4	0.1308	0.1235	0.0001
(BG)1	0.3103	0.3074	0.0001
(BG)2	0.3378	0.3322	0.0001
(GG)3	0.3529	0.3447	0.0001
(BG)4	0.3660	0.3553	0.0001
(BGW)1	0.3218	0.3175	0.0001
(BGW)2	0.3491	0.3409	0.0001
(GGW)3	0.3675	0.3579	0.0001
(BGW)4	0.3888	0.3682	0.0001

The numbers following the B, G, and/or W (e.g. B1, B2, etc.) indicates the number of images used. The statistics for R^2, adjusted R^2 and the P-value are the average of all possible combinations at a given number of images for the regression. The total number of plots used is 481 for stands ranging from 20 to 300+ years old. We removed the first two age classes for analysis because the stand age classes do not apply to the 1984 image.

according to stand age (Fig. 4). The decreasing trend in brightness with stand age derived from FIA plots is obvious (Fig. 4a), however we do not see a rapid decrease in brightness during the early years of succession as observed in our simulation. This difference between the real and simulated trajectories is likely a result of the simulation trajectories starting on a bright, bare soil background, while the youngest FIA stands (class code 1, ages 0–9) could have varying amounts of vegetation already established. In addition, the decadal averaging in the observed succession trajectories also reduced the rate of change with time.

The observed greenness trajectory with stand age resembles that from simulation, i.e. greenness increases with stand age initially and then decreases as the stand becomes older (Fig. 4b). The maximum greenness for a stand is around 30 years of age. Again the nonlinearity in greenness in the early years of succession as seen in the simulation is significantly dampened in the regional mean greenness trajectory. Wetness increases with stand age rapidly in the early years (Fig. 4c), then we do not see a clear trend after 40 years. For all three real Tasseled Cap trajectories, there are high uncertainties associated with stand age. As the stands get older, the uncertainty tends to decrease. However, the trajectories of the mean values of all stands in the region match with the simulation well for brightness and greenness, but no clear decreasing trend in wetness as simulated can be seen from the observed data from mature and old-growth stands. Due to the subtlety in the decreasing trend of wetness in the simulation from mature and old-growth stands, the difference in the rate of regeneration for stands in the Coastal Ranges and western Cascades (Yang et al., 2005) may obscure the trend. We examined the trend of wetness with stand age for stands in the two regions separately (Fig. 5). The decreasing trend of wetness with stand age for mature and old-growth stands is much clearer when viewed separately for the Coastal Ranges and western Cascades. Therefore, the temporal trajectory of wetness index is more sensitive to the scale of aggregation of ecoregions than brightness and greenness. This is probably due to the fact that information

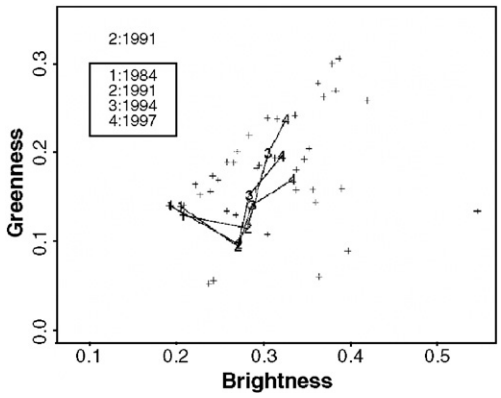

Fig. 6. Spectral history for age class 1 stands in the brightness/greenness space in the 1984 image, indicating that some stands were clear cut between 1984 and 1991. Stand age classes 1 and 2 in the FIA dataset will not apply to the 1984 image. Similar problem can occur to some plots in other age classes in 1997 image because such change could happen during the time between FIA data collection and image acquisition. These stands can be identified and removed from statistical analysis.

Table 4
Results of multiple regression analysis between age classes and brightness (B), greenness (G) and wetness (W) indices from 1984, 1991, 1994 and 1997 Landsat 5 TM images for all plots after screening

Variables	R^2	Adj R^2	P-value
B1	0.4674	0.4662	0.0001
B2	0.4944	0.4920	0.0001
B3	0.5118	0.5083	0.0001
B4	0.5242	0.5197	0.0001
G1	0.4573	0.4560	0.0001
G2	0.4929	0.4906	0.0001
G3	0.5051	0.5015	0.0001
G4	0.5114	0.5067	0.0001
W1	0.0694	0.0597	0.0307
W2	0.1146	0.1104	0.0002
W3	0.1598	0.1538	0.0001
W4	0.2018	0.2018	0.0001
(BG)1	0.4875	0.4850	0.0001
(BG)2	0.5151	0.5105	0.0001
(BG)3	0.5287	0.5219	0.0001
(BG)4	0.5382	0.5293	0.0001
(BGW)1	0.4983	0.4947	0.0001
(BGW)2	0.5318	0.5245	0.0001
(BGW)3	0.5449	0.5350	0.0001
(BGW)4	0.5564	0.5435	0.0001

The numbers following the B, G, and/or W (e.g. B1, B2, etc.) indicates the number of images used. The statistics for R^2, adjusted R^2 and the P-value are the average of all possible combinations at a given number of images for the regression. The total number of plots used is 424 for stands ranging from 20 to 300+ years old. We removed the first two age classes for analysis because the stand age classes do not apply to the 1984 image, and the plots with change occurred during the period from ground data collection and image acquisition.

content or percent image variation accounted for by wetness is much lower than brightness and greenness. Thus the wetness has a lower signal to noise ratio, making wetness pattern more sensitive to noise.

3.3. Statistical analysis

Because the FIA data were collected between 1995 and 1997 in our study area (Hiserote & Waddell, 2004), we do not have age information for young stands prior to the current stand conditions. Therefore, we excluded the stands in the first two age classes (i.e. age <20 years old) from our statistical analysis. This would also eliminate most of the initial nonlinear effects of stand age on remote sensing signals. We continue to use stands on sites with slopes less than 30° and below 1000 m of elevation in the analysis to reduce topographic effects. Table 3 shows the results of regression analysis between stand age and Tasseled Cap spectral indices for all 481 plots. Though the overall adjusted R^2 values are relatively low, the relationship between stand age and the spectral signals are extremely significant, except for wetness. The low adjusted R^2 for wetness is understandable given the ambiguous pattern observed (see Fig. 4c). The adjusted R^2 values increase steadily with the number of images for brightness, greenness and wetness. Due to the fact that surface conditions may change after FIA data collection and before image acquisition, there still exist stands whose ages in FIA do not match the actual ages for stands in the image. These stands can be eliminated based on its spectral history as seen in Fig. 6. If there is a sudden increase in brightness and decrease in greenness or sudden increase in both greenness and brightness for mature and old-growth stands, these stands are considered as experienced change and are eliminated from statistical analysis. After eliminating these stands, we have a total of 424 stands left. Table 4 shows the results of regression analysis equivalent to Table 3, but the overall adjusted R^2 values increased significantly. The basic pattern still remains: (1) the more images we use, the higher the adjusted R^2; (2) brightness and greenness have much stronger relationship with stand age than wetness. The magnitude of increase in R^2 is greatest from one to two images. Further increase in the number of images has much smaller magnitude of increase in R^2. This may be due to the limited time span in the four images. Once two of the images are used, an addition of another image close in time may not add much new information.

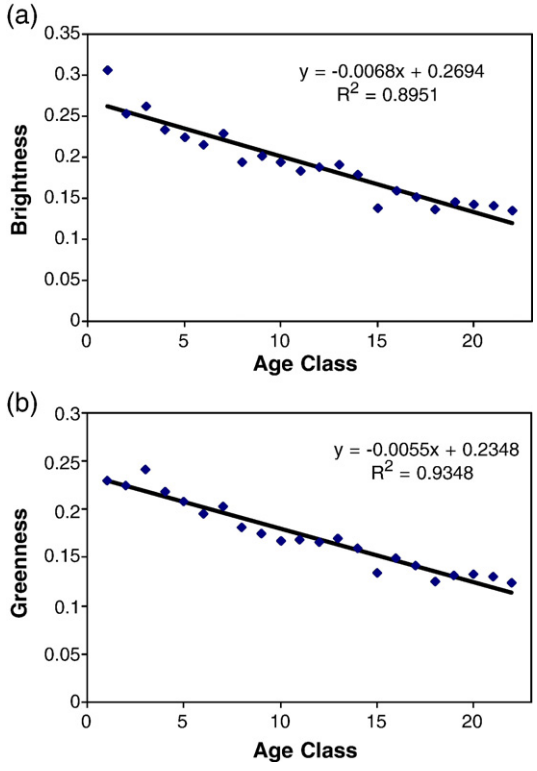

Fig. 7. A linear model fits the regional mean succession trajectories in (a) brightness and (b) greenness well with the 1997 image. Note points in this Figure are the same points as seen in Fig. 4(a, b). The large cross-site variation almost masked the nonlinearity at individual stand scale.

4. Discussions

Our analysis clearly identified the synergistic value of using multitemporal Landsat imagery to predict distributions of forest succession from young to old-growth stages. However, the overall adjusted R^2 values are relatively low. It seems that there are several reasons for the low adjusted R^2 values that are beyond the control of this study. First, the locational accuracy for the stands is unknown to us. Because we are working on the scale of 30 × 30 m pixels, locational error can cause mismatch of plots on the ground with the stand in the image, reducing the goodness of fit between remote sensing signals and stand ages. Second, the accuracy of stand ages is unknown to us. Errors in age class can weaken the relationship between remote sensing signals and stand ages. Finally, there are natural variations in composition and structure for a given stand age resulting from variations in site conditions (Fig. 4). Over a large geographic areas, the natural variation of the physical structure at a given age class can be significant (Yang et al., 2005). We further tested whether a linear model as Eq. (5) is a valid model. Fig. 7 shows that a linear model fits well for the regional mean successional trajectories for brightness and greenness with the 1997 image. We also did a comparison of a linear with a nonlinear (regressing age with natural log of brightness) model for brightness using 1997 data with 424 plots, the two models produced almost identical R^2 values, indicating cross-site variations masked the nonlinear effects when successional trajectories are constructed via substituting space for time. Fig. 4c clearly indicates that a linear model does not fit the trajectory of wetness. Though our simulation captured the regional average trend of forest succession in optical imagery, it is far from operational in mapping forest stand ages on a stand basis with reasonable accuracy due to the large uncertainties associated with forest succession trajectories and the relatively low R^2 values shown in Table 4. To make matters more complex, the spectral trajectories produced are applicable to conifer stands only. Therefore, our approach may not be applicable to broad leaf stands or stands with significant mixture of broad leaf and conifer trees.

Several earlier studies in western Oregon found that the Tasseled Cap wetness index is the most effective spectral index for mapping age class information for closed canopy conifer stands (Cohen & Spies, 1992; Cohen et al., 1995; Fiorella & Ripple, 1993). Results of our analysis differ from these earlier observations in that brightness and greenness both have much higher adjusted R^2 values than wetness. This is likely due to including both open and closed canopy stands in this analysis, as well as the potential spectral heterogeneity contained within the FIA plot data. Among the three Tasseled Cap indices, wetness has the lowest information content (or percent image variation contained) compared to brightness and greenness (Cohen et al., 1995). The noise level in the age class information is perhaps too high to allow the effect of wetness to be captured from FIA plots. Therefore, our study found that the relationship between Tasseled Cap indices and stand ages with FIA plots is more complex than the literature has previously indicated.

5. Conclusions

This study produced successional trajectories from young to old-growth stages based on ecological principals and radiation physics by coupling a forest succession model (ZELIG) with a canopy reflectance model (GORT). The successional trajectories produced by the ZELIG-GORT simulation captured the major characteristics of the observed regional mean trajectories for Tasseled Cap indices. Young closed canopy stands have the highest greenness and wetness values. Further development leads to a slow decrease in brightness, greenness and wetness values from mature to old-growth stages with the decrease in wetness displaying the smallest magnitude. Though the simulated successional trajectory of an individual stand is quite nonlinear, particularly in the first 30 years of development, a linear model fits the regional average succession trajectory quite well due to large cross-site variation that masked the nonlinearity. Our study found that Tasseled Cap brightness and greenness are much better predictors of forest successional stages than wetness index is. The temporal pattern of regional mean wetness trajectory is more sensitive to the scale of ecoregion aggregation than brightness and greenness. The spectral history based on multitemporal Landsat imagery can effectively enhance data quality in monitoring forest succession with remote sensing. Multiple regression analysis based on individual stands indicates that multitemporal Landsat imagery improves prediction of distributions of forest succession from young to old-growth stages. However, the highest adjusted R^2 using all four images in this study is 0.54 for 20 age classes due to large variation of remote sensing signals at the same successional stages. Therefore, site-specific factors influencing canopy reflectance need to be accounted for in order to predict forest successional stages more accurately at individual stands in the future.

Acknowledgements

The authors thank Dr. Curtis E. Woodcock at Boston University for useful discussions at the early stage of the development of this paper, and Dr. Robert Kennedy at the Forest Sciences Laboratory, Oregon State University for help with slope and aspect conversions for FIA plots. The authors gratefully acknowledge data, interpretive assistance and financial support provided by the USDA Forest Service Pacific Northwest Research Station's Forest Inventory and Analysis Program. This research was partly supported by NSF Grant 0351430. The initial manuscript was completed while Dr. Conghe Song was a Charles Bullard Fellow in Forest Research at Harvard Forest, Harvard University during 09/01/05–05/31/06.

References

Botkin, D. B., Janak, J. F., & Wallis, J. R. (1972). Rationale, limitations, and assumptions of a northeastern forest growth simulator. *IBM Journal of Research and Development*, *16*, 101−116.

Chavez Jr., P. S., (1996). Image-based atmospheric corrections-revisited and improved. *Photogrammetric Engineering and Remote Sensing*, *62*, 1025−1036.

Chen, W. J., Chen, J. M., Price, D. T., & Cihlar, J. (2002). Effects of stand age on net primary productivity of boreal black spruce forests in Ontario, Canada. *Canadian Journal of Forest Research*, *32*(5), 833−842.

Cohen, W. B., & Spies, T. A. (1992). Estimating structural attributes of Douglas-fir western Hemlock forest stands from Landsat and spot imagery. *Remote Sensing of Environment*, *41*(1), 1−17.

Cohen, W. B., Fiorellan, M., Gray, J., Helmer, E., & Anderson, K. (1998). An efficient and accurate method for mapping forest clearcuts in the Pacific Northwest using Landsat Imagery. *Photogrammetric Engineering and Remote Sensing*, *64*(4), 293−300.

Cohen, W. B., Spies, T. A., Alig, R. J., Oetter, D. R., Maiersperger, T. K., & Fiorella, M. (2002). Characterizing 23 years (1972–95) of stand replacement disturbance in western Oregon forests with Landsat imagery. *Ecosystems*, *5*, 122−137.

Cohen, W. B., Spies, T. A., & Fiorella, M. (1995). Estimating the age and structure of forests in a multi-ownership landscape of western Oregon, USA. *International Journal of Remote Sensing*, *16*, 721−746.

Crist, E. P. (1985). A TM Tasseled Cap equivalent transformation for reflectance factor data. *Remote Sensing of Environment*, *17*, 301−306.

Dixon, R. K., Brown, S., Houghton, R. A., Solomon, A. M., Trexler, M. C., & Wisniewski, J. (1994). Carbon pools and flux of global forest ecosystems. *Science*, *263*, 185−190.

Dobson, A. P., Bradshaw, A. D., & Baker, A. J. M. (1997). Hopes for the future: restoration ecology and conservation biology. *Science*, *277*, 515−522.

Fiorella, M., & Ripple, W. J. (1993). Determining successional stage of temperate coniferous forests with Landsat satellite data. *Photographic Engineering and Remote Sensing*, *59*, 239−246.

Foody, G. M., Palubinskas, G., Lucas, R. M., Curran, P. J., & Honzak, M. (1996). Identifying terrestrial carbon sinks: classification of successional stages in regenerating tropical forest from Landsat TM data. *Remote Sensing of Environment*, *55*, 205−216.

Goodale, C. L., Apps, M. J., Birdsey, R. A., Field, C. B., Heath, L. S., Houghton, R. A., et al. (2002). Forest carbon sinks in the Northern Hemisphere. *Ecological Applications*, *21*, 891−899.

Hall, F. G., Botin, D. B., Strebel, D. E., Woods, K. D., & Goetz, S. J. (1991). Large-scale patterns of forest succession as determined by remote sensing. *Ecology*, *72*(2), 628−640.

Hiserote, B., & Waddell, K. (2004). *The PNW-FIA integrated database user guide version 1.4.* Portland, OR: Forest Inventory and Analysis Program, Pacific Northwest Research Station.

Jakubauskas, M. E. (1996). Thematic mapper characterization of lodgepole pine seral stages in Yellowstone National Park, USA. *Remote Sensing of Environment*, *56*, 118−132.

Kaufman, Y. J., Tanre, S., Remer, L. A., Vermote, E. F., Chu, A., & Holben, B. N. (1997). Operational remote sensing of tropospheric aerosol over land from

EOS moderate resolution imaging spectroradiometer. *Journal of Geophysical Research*, *102*(D14), 17,051−17,067.

Kauth, R. J., & Thomas, G. S. (1976). The tasseled cap — a graphic description of the spectral–temporal development of agricultural crops as seen by Landsat. *Proceedings on the symposium on machine processing of remotely sensed data, 4b: 41–51, 6 June–2 July, 1976, West Lafayette, Indiana*.

Kimes, D. S., Holben, B. N., Nickeson, J. E., & McKee, W. A. (1996). Extracting forest age in a pacific northwest forest from Thematic Mapper and topographic data. *Remote Sensing of Environment*, *56*, 133−140.

Lal, R. (1997). Deforestation effects on soil degradation and rehabilitation in western Nigeria. 4. *Hydrology and Water Quality, Land Degradation and Development*, *8*(2), 95−126.

Li, X., & Strahler, A. H. (1985). Geometric-optical modeling of a conifer forest canopy. *IEEE Transactions on Geoscience and Remote Sensing*, *GE-23*, 705−721.

Li, X., & Strahler, A. H. (1992). Geometric-optical bidirectional reflectance modeling of the discrete crown vegetation canopy: effect of crown shape and mutual shadowing. *IEEE Transactions on Geoscience and Remote Sensing*, *30*, 276−292.

Li, X., Strahler, A. H., & Woodcock, C. E. (1995). A hybrid geometric optical-radiative transfer approach for modeling albedo and directional reflectance of discontinuous canopies. *IEEE Transactions on Geoscience and Remote Sensing*, *33*, 466−480.

Liang, S., Fallah-Adl, H., Kalluri, S., JaJa, J., Kaufman, Y. J., & Townshend, J. R. G. (1997). An operational atmospheric correction algorithm for Landsat Thematic Mapper imagery over the land. *Journal of Geophysical Research*, *102*, 17,173−17,186.

Lucas, R. M., Honzak, M., DO Amaral, I., Curran, P. J., & Foody, G. M. (2002). Forest regeneration on abandoned clearances in central Amazonia. *International Journal of Remote Sensing*, *23*(5), 965−988.

Pax-Lenney, M., Woodcock, C. E., Macomber, S. A., Gopal, S., & Song, C. (2001). Forest mapping with a generalized classifier and Landsat TM Data. *Remote Sensing of Environment*, *77*, 241−276.

Pregitzer, K. S., & Euskirchen, E. S. (2004). Carbon cycling and storage in world forests: biome patterns related to forest age. *Global Change Biology*, *10*(12), 2052−2077.

Schott, J. R., Salvaggio, C., & Volchok, W. J. (1988). Radiometric scene normalization using pseudoinvariant features. *Remote Sensing of Environment*, *26*, 1−16.

Serra, J. (1980). The Boolean model and random sets. *Computer Graphics and Image Processing*, *12*, 99−126.

Shugart, H. H., & West, D. C. (1977). Development of an Appalachian deciduous forest succession model and its application to assessment of the impact of the chestnut blight. *Journal of Environmental Management*, *5*, 161−179.

Skole, D., & Tucker, C. (1993). Tropical deforestation and habitat fragmentation in the Amazon: satellite data from 1978 to 1988. *Science*, *260*, 1905−1910.

Song, C., & Woodcock, C. E. (2003). The importance of landuse history and forest age structure in regional terrestrial carbon budgets. *Ecological Modelling*, *64*, 33−47.

Song, C., & Woodcock, C. E. (2003). Monitoring forest succession with multitemporal Landsat images: factors of uncertainty. *IEEE Transactions on Geoscience and Remote Sensing*, *41*(11), 2557−2567.

Song, C., Woodcock, C. E., & Li, X. (2002). The spectral/temporal manifestation of forest succession in optical imagery: the potential of multitemporal imagery. *Remote Sensing of Environment*, *82*, 286−303.

Song, C., Woodcock, C. E., Seto, K. C., Pax-Lenney, M., & Macomber, S. A. (2001). Classification and change detection using Landsat TM Data: when and how to correct atmospheric effects? *Remote Sensing of Environment*, *75*, 230−244.

Urban, D. L. (1990). *A versatile model to simulate forest pattern: a user's guide to ZELIG version 1.0.* Charlottesville, Virginia: University of Virginia.

Urban, D. L., Harmon, M. E., & Halpern, C. B. (1993). Potential response of pacific northwestern forests to climatic-change, effects of stand age and initial composition. *Climatic Change*, *23*(3), 247−266.

Vermote, E. F., Tanre, D., Deuze, J. L., Herman, M., & Morcrette, J. J. (1997). *Second simulation of the satellite signal in the solar spectrum (6S), 6S user's guide version 2.* Greenbelt, Maryland 20771,USA: NASA Goddard Space Flight Center, Code 923.

Wofsy, S. C., Goulden, M. L., Munger, J. W., et al. (1993). Net exchange of CO_2 in a midlatitude forest. *Science*, *260*, 1314−1317.

Woo, M. K., Fang, G. X., & DiCenzo, P. D. (1997). The role of vegetation in the retardation of soil erosion. *CATENA*, *29*(2), 145−159.

Yang, Z., Cohen, W. B., & Harmon, M. E. (2005). Modeling early forest succession following clear-cutting in western Oregon. *Canadian Journal of Forest Research*, *35*, 1889−1900.